Available online at www.sciencedirect.com

ScienceDirect

Solar Energy 115 (2015) 505–517

SOLAR ENERGY

www.elsevier.com/locate/solener

Assessment of a falling solid particle receiver with numerical simulation

Birgit Gobereit [a,*], Lars Amsbeck [b], Reiner Buck [b], Robert Pitz-Paal [c], Marc Röger [d], Hans Müller-Steinhagen [e]

[a] German Aerospace Center (DLR), Institute of Solar Research, Point Focusing Systems, Pfaffenwald-Ring 38-40, 70659 Stuttgart, Germany
[b] German Aerospace Center (DLR), Institute of Solar Research, Stuttgart, Germany
[c] German Aerospace Center (DLR), Institute of Solar Research, Cologne, Germany
[d] German Aerospace Center (DLR), Institute of Solar Research, Almería, Spain
[e] Technische Universität Dresden, Germany

Received 7 October 2014; received in revised form 4 March 2015; accepted 7 March 2015
Available online 30 March 2015

Communicated by: Associate Editor Yogi Goswami

Abstract

An advanced computational fluid dynamics (CFD) model was developed which allows detailed analysis of a direct absorption falling particle receiver with horizontal aperture (face down) for a solar tower plant. The CFD model includes all relevant effects: movement of the particle curtain and the air, solar radiation, thermal radiation transfer, mechanical and thermal interactions between the particles, the air and the walls and conduction through the walls. These are spatially resolved in three dimensions for the complete receiver including the surrounding air. The coupled equations for thermal radiation, conduction and convective heat transfer are solved iteratively. First results are compared with previous simulations with a simple Matlab model and the differences due to the improvements in the simulations are discussed.

The receiver efficiency was determined to be 83% at the design point (400 MW solar input) using a single drop (no recirculation) to heat the particles from 300 °C to 800 °C. In contrast, by separating the circumferential particle curtain into 4 parts and recirculating the particles 3 times through all the sections in series the receiver efficiency increases to more than 92%. This is due to lower reflection losses from the higher particle mass flow and therefore higher opacity of the particle curtain.

Wind effects have been studied for the cylindrical face down receiver for the 100% load case with only one recirculation. For 15 m/s horizontal wind speed the receiver efficiency reduces from 89% to 84%.

Keywords: Concentrated solar power (CSP); Solid particle receiver; Direct absorption; Numerical fluid dynamics simulation

1. Introduction

A first campaign to develop a falling particle receiver for solar tower plants was led by Sandia in the 1980s (Falcone et al., 1982, 1985). A cavity receiver was proposed through which particles fall freely. In this conceptual design, the falling particles form a particle curtain that is irradiated directly by the concentrated solar radiation. First model prediction, a screening of particulate materials, and cost and system analyses were presented. This work already envisaged particle power plants for electricity generation, as shown in Fig. 1. Particles are lifted up to a tower receiver for solar heating and then back down to a hot storage on the ground. The hot particles can be used on demand to supply heat to a process. A cold storage completes the

* Corresponding author. Tel.: +49 (0)711 6862 519.
E-mail address: birgit.gobereit@dlr.de (B. Gobereit).

http://dx.doi.org/10.1016/j.solener.2015.03.013
0038-092X/

Nomenclature

A	area, m^2
E	specific emission, W/m^2
F	force, N
g	gravity, 9.81 m/s^2
h	heat transfer coefficient, $W/(m^2K)$
I	intensity, W/m^2
K	absorption coefficient
m	mass, kg 1/m
$\dot{m}$	mass flow, kg/s
p	pressure, Pa
$\dot{Q}$	energy flow, W
s, x	length, location, m
t	time, s
T	temperature, K
v	velocity, m/s
η	efficiency –
ε	emissivity –
μ	dynamic viscosity, Pa s
σ	density, kg/m^3

Dimensionless quantities

Ma	Mach-Number
Nu	Nusselt-Number
Pr	Prandtl-Number
Re	Reynolds-Number

Subscripts

a	air
DP	design point
in	incoming
n	in time step n
p	particles
rec	receiver

loop. The lift system was supposed to be based on a mine hoist with an insulated skip.

In a falling particle receiver nearly black particles are dropped inside a cavity to directly absorb the concentrated solar radiation. Sand-like ceramic particles with a diameter between 0.3 and 2 mm are considered as sufficient. Ceramic bauxite particles, usually used in fracking deep wells by the oil and gas industry, can be used up to 1000 °C, are nearly black (Griffin et al., 1986), available in large quantities and cost around the same as $NaNO_3/KNO_3$ (500–1000 €/t).

A first prototype of a falling particle receiver was tested over a range of input power levels from 1.58 to 2.51 MWth to provide experimental data for model validation (Siegel et al., 2010). A particle temperature increase up to 250 °C was demonstrated. CFD simulation and experimental results showed good agreement.

Other previous experimental and theoretical studies of particle flow (Kim et al., 2010b), wind effects (Kim et al., 2010a; Tan et al., 2009) and thermal simulation (Grena, 2009) can be found in literature.

Ceramic particles open the possibility to drive processes, which need higher temperatures than state-of-art molten salt systems can achieve, while still including an inherent storage capability. The most efficient steam turbines feature 620 °C reheated steam today. Supercritical CO_2 and gas turbine cycles as well as industrial thermal processes other than electricity production can also be considered. ALSTOM proposed a circulating moving bed combustion system. In this system high-density solid particles are heated by the combustion products while falling downward through the upper region of a combustor. The particles are transferred to a moving bed heat exchanger (MBHE). Proof of concept tests were successfully performed with 7000 µm bauxite particles at ALSTOM's 3 MWth test facility (Jukkola et al., 2003). Direct contact heat exchange with air being blown through a moving particle bed could also

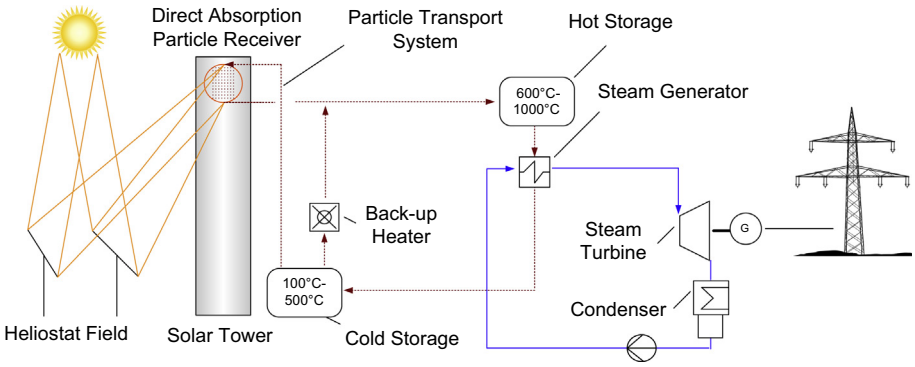

Fig. 1. Solar power plant with particle receiver, steam turbine and back-up heater.

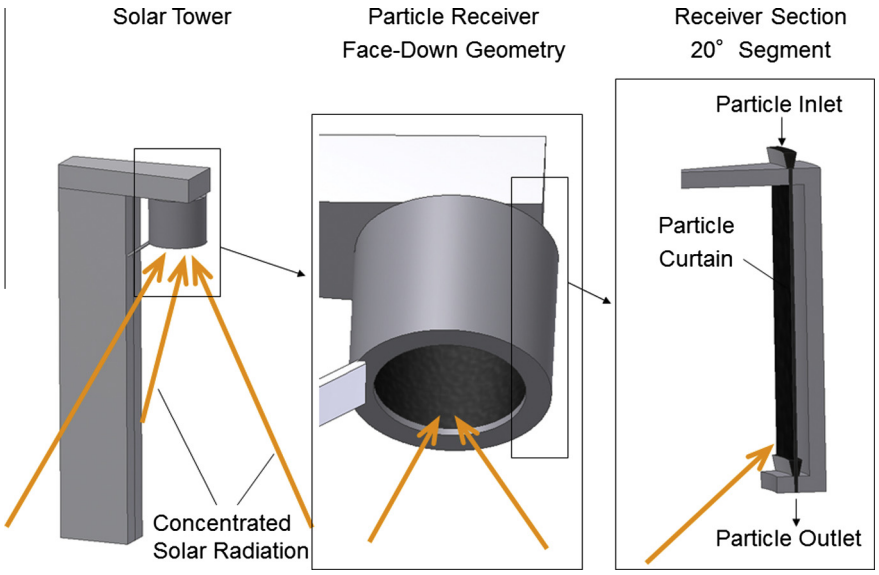

Fig. 2. Solar power tower with face down cavity (left); face down cavity with particle curtain, view from below (middle); segment of cavity and particle curtain (right).

be an efficient and economical way, especially via hybridization of atmospheric combustion.

A schematic representation of a power tower with a horizontal aperture (face down) cavity receiver is shown in Fig. 2. Receiver losses are minimized with such a receiver configuration. Due to the cavity effect reflection losses are reduced. Since a dedicated absorption structure is not necessary, thermal radiation is reduced, while allowing very high solar flux density. The horizontal, downwards facing aperture leads to low convection losses without requirement for a window or other additional efforts like an air curtain. The simple structure and absence of expensive high temperature alloys offer furthermore the possibility of low receiver costs.

Hence, high receiver efficiency at high outlet temperature and therefore high overall efficiency seem to be feasible. A detailed receiver model was developed to show that these basic considerations can be confirmed theoretically. The key points for a modeling method are presented and its advancements beyond the state of the art are discussed.

2. Modeling of falling particle receiver – previous work

Preliminary work involving different modeling approaches indicated high receiver efficiencies. A simple screening Matlab model and a computational fluid dynamics model have so far been presented (see e.g. Ho et al., 2009; Siegel et al., 2010).

The Matlab model (Röger et al., 2011) simulates mainly the radiative heat transfer in the receiver cavity using view factors and effective radiative properties of the wall or curtain surfaces. It simplifies the particle curtain to front and back faces, connected by heat conduction and effective optical properties. These properties include all internal curtain effects like absorption or multiple reflections and are based on correlations, like drag force plus the assumption of the entrained air velocity being 70% of the particle velocity. Distribution of solar radiation on the surface elements is determined by ray-tracing methods. Convective losses are added via a simplified correlation after detailed receiver modeling. The model was validated for a flat particle curtain in a cavity with north-facing aperture at temperatures of up to 250 °C (Ho et al., 2009). It was used to simulate a face-down receiver and to determine an efficient recirculation scheme (Röger et al., 2011). To consider the interaction between particles and air as well as convective streaming within the cavity, fluid dynamic simulations are required.

Recirculation is an operation mode to raise the temperature by returning the heated particles back to the inlet and dropping them more than once through the receiver. The reason for this operation mode is to yield high receiver efficiency with a particle outlet temperature of 800 °C in part load (solar input power lower than design point).

Fig. 3 shows a schematic to explain the benefit of recirculation. On the left hand, design point condition with one pass of the particles is shown. The particles enter the receiver at the inlet temperature T_{in} with a particle mass flow $\dot{m}_{DP}$. The concentrated solar radiation heats them to the outlet temperature T_{out}. A part of the radiation is transmitted through the curtain and is reflected by the back walls. Common ceramic insulation material has a reflectivity of about 80%. Thus, the walls reflect the larger part of the transmitted radiation. A portion of the reflected radiation is lost by passing through the curtain and leaving the receiver.

Solar radiation varies with time, thus outlet temperature changes using a one-pass operation method. In order to provide a constant temperature to the storage and the

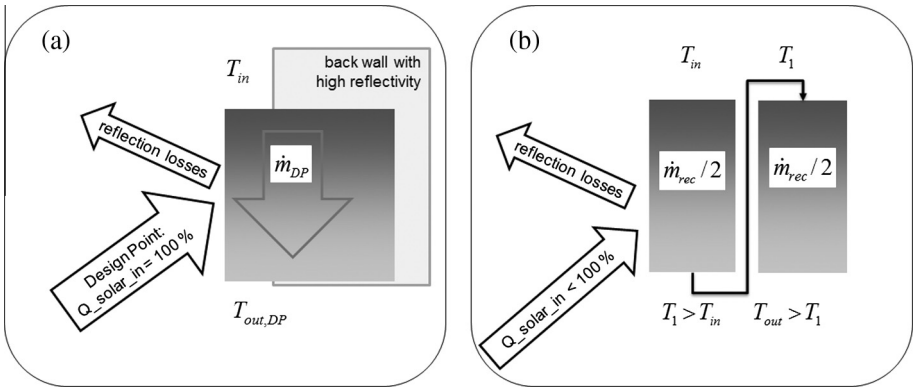

Fig. 3. (a) Design point (DP) conditions, (b) part load with one recirculation.

power block, an adjustment of the outlet temperature is desired. This can be realized by adapting the particle mass flow to the solar input power. Without recirculation this will lead to a more transparent particle curtain and therefore to higher reflection losses.

To obtain the desired outlet temperature and high receiver efficiency (low reflection losses), serial recirculation is an adequate operation strategy (Röger, 2001). Serial recirculation means that the particle curtain is divided into two or more parts. The first part consists of the particles during the first drop, which are collected at the bottom. The particles then drop a second time in the second part of the curtain, parallel to the first one (see Fig. 3b). If needed, more parts can be added and the procedure is repeated accordingly. Hence, overall particle mass flow in the receiver $\dot{m}_{rec}$ is higher than effective mass flow. Effective mass flow is the amount of particle that enters the receiver with the initial temperature and leaves the receiver at the outlet temperature. To be able to compare the results, specific particle mass flow is an adequate quantity, which is the overall particle mass flow in the receiver $\dot{m}_{rec}$ divided by the length of the inlet slot (opening of the inlet hopper, through which the particles enter the receiver).

Ho et al. presented a FLUENT model, which solves the fluid dynamic equations and calculates the particles using a Euler–Lagrange method. The particle curtain is modeled without consideration of the depth of the particle curtain. The new modeling approach however discretizes the particle curtain in three dimensions. The variation of variables with the depth of the particle curtain is also resolved.

Incoming solar radiation is determined with Monte Carlo ray-tracing using a "solar patch". This solar patch is a 2D-location of the simulation domain, located in the aperture and radiating with different intensities into different solid angles. Further radiation modeling is done in FLUENT. In the presented new model, ray-tracing is determined until absorption in the particles or on the wall occurs, or the ray leaves the cavity.

The aperture is modeled with an "opening boundary", which means 0-bar pressure difference and a fixed temperature. Therefore, a flow field in the aperture will not be simulated with fluid dynamics. Boundary conditions are set at this face, which might yield to unrealistic flow conditions, for example hot exiting air streams result in cold entering air streams. To avoid this, the present model also includes the surrounding air.

So far, only simulation results for a flat or C-shaped particle curtain in a cavity with sideways open aperture are available. Therefore, simulation results of the model presented in this paper are compared to the Matlab results (Ho et al., 2009; Siegel et al., 2010).

3. Methodology

An advanced model was developed to assess all significant physical effects in the face down particle receiver. The model takes into account solar radiation, particle movement, radiative and convective heat transfer, fluid dynamics in the air as well as wind effects. Major improvements are including the surrounding air and a particle curtain, which is spatially resolved in three dimensions. The modeling results are benchmarked with the results from the Matlab model.

3.1. Modeling tools and coupling

The air in the cavity and in the surrounding is modeled with computational fluid dynamics (CFD). Steady-state was assumed for the simulations. For particle simulation the Euler–Lagrange approach was used. This was modeled with commercial software (ANSYS, 2009). Solar radiation was modeled with ray-tracing software (SPRAY based on MIRVAL (Buck and Teufel, 2009; Leary and Hankins, 1979)). The ray-tracing software was enhanced to take into account volumetric absorption in the particle curtain.

The two models were coupled iteratively, which is shown in Fig. 4. First, several input parameters have to be set, such as location, design point, receiver geometry, material properties of receiver walls and particles.

The heliostat field layout was calculated using HFLCAL (Schwarzbözl et al., 2009). CFD simulation using Euler–

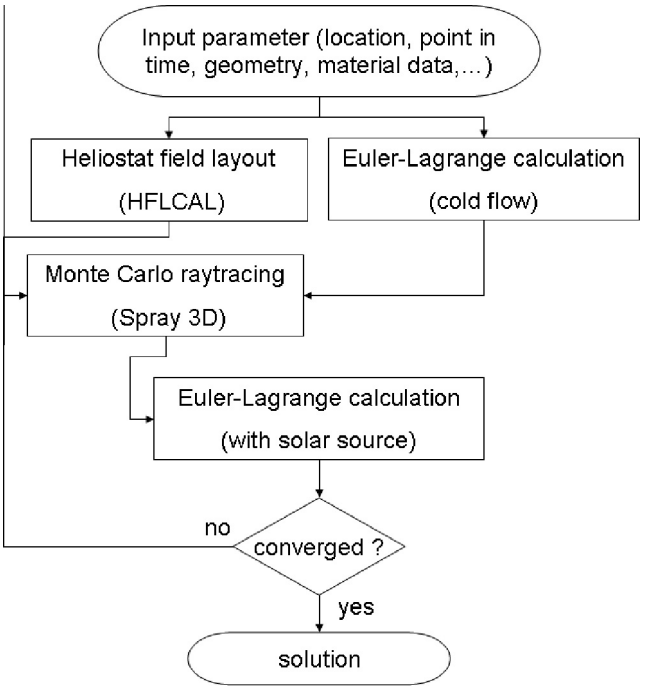

Fig. 4. Coupling between CFD simulation and solar ray-tracing model.

Lagrange model provide initial particle distribution. Heliostat field and particle distribution are then fed into ray-tracing simulation.

Ray-tracing returns heat sources for particles and flux densities for receiver walls. These are used as boundaries in the subsequent CFD simulation. As the particle distribution might change due to heating, ray-tracing has to be repeated with the new particle distribution. Iteration between CFD and ray-tracing is conducted until a converged solution is found.

3.2. Domain and boundaries

To ensure that the air flow through the aperture was simulated properly, the surrounding of the cavity was also modeled. It is divided into two parts (see Fig. 5). For cases without wind the solution of simulations including the outer surrounding were compared to simulations including only the inner surrounding. Differences in convective losses between both results were below 1%. Therefore, for cases without wind the simulation domain was reduced to the cavity and the inner part of the surrounding. Opening boundary conditions have been chosen for all the boundary faces of the surrounding. This means a fixed temperature of 27 °C and a 0 bar pressure difference condition, regarding the reference pressure of 1 atm.

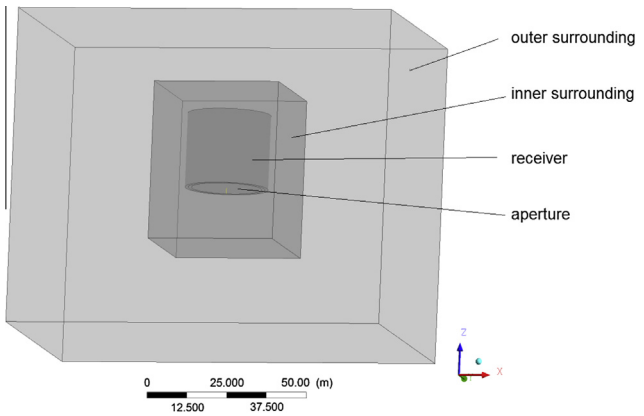

Fig. 5. Domain for CFD simulation.

When wind is simulated, the outer surrounding is included, to avoid an influence of the boundaries on the solutions. An adequate size of the domain was determined by analyzing different sizes. The wind was modeled with an inlet boundary, with a horizontal flow direction and a fixed inlet velocity at one side of the outer surrounding. For the inlet flow a medium turbulence intensity of 5 % and an eddy viscosity ratio of 10 were assumed at the boundary, and are computed locally during the simulations in the whole domain.

Cavity walls are assumed to be insulated and heat loss via receiver walls is modeled corresponding to 50 mm insulation with a thermal conductivity of 0.055 W/m K. A constant heat transfer coefficient of 5 W/m^2/K was assumed at the outside of the cavity. This was implemented with a simplified approach (heat sink temperature 27 °C, fixed heat transfer coefficient of 0.9061 W/m^2 K).

3.3. Modeling of air flow

For the presented case, Navier–Stokes equations are used to model fluid flow, with the time and space dependent variables: velocity $\vec{v}$, density ρ, pressure p, which describes fluid flow, the dynamic viscosity μ and gravity $\vec{g}$.

$$\rho\left(\frac{\partial \vec{v}}{\partial t} + (\vec{v}\nabla)\vec{v}\right) = -\nabla p + \mu\Delta\vec{v} + \vec{g}\rho \quad (1)$$

Air is modeled as incompressible medium since Ma < 1 while density varies with temperature, resulting in the following continuity equation:

$$\frac{\partial \rho}{\partial t} + \nabla(\rho\ \vec{v}) = 0 \quad (2)$$

Shear Stress Transport (SST) model is used for turbulence phenomena, since it is the most appropriate available turbulence model. Herein the commonly used k– ε- and k– ω -models are combined, which yields to more accurate determination of turbulence (Menter et al., 2003). Regions near walls are modeled by wall functions.

3.4. Modeling of particles and coupling

We compute air–particle interaction using the Euler–Lagrange method. Particles are simulated along particle tracks. The displacement of particles during a time step δt is given by the general equations for accelerated movement:

$$\vec{x}_{n+1} = \vec{x}_n + \vec{v}_p \delta t \tag{3}$$

Particle velocity $\vec{v}_p$ can be determined from particle mass m_p and the sum of all acting forces $\sum F_i$:

$$m_p \frac{d\vec{v}_p}{dt} = \sum F_i \tag{4}$$

Only gravity and drag are considered. Particle–particle interaction is neglected, because the particle volume fraction is low ($\ll$10%). Other forces, like system rotation, added mass or pressure gradient are not significant, and not considered in the model. The simulation is fully coupled, i.e. the continuous flow is affected by the particles, and the particles are affected by the continuous flow.

Drag can be computed with the Schiller–Naumann equation (VDI, 2006), that was extended to fit a wide range of Reynolds-Numbers ($0.1 < \mathrm{Re} < 1 \times 10^5$):

$$C_D = \max\left(\frac{24}{\mathrm{Re}}\left(1 + 0.15\mathrm{Re}^{0.687}\right)\ ,\ 0.44\right) \tag{5}$$

For the presented simulation, the particles are considered to be spherical.

Ranz–Marshall correlation (Crowe et al., 1997) is used to calculate heat transfer:

$$Nu = 2 + 0.6\mathrm{Re}_P^{0.5}\mathrm{Pr}^{0.3} \tag{6}$$

It is valid for $0 < \mathrm{Pr} < 0.7$ and $0 < \mathrm{Re}_p < 200$, where Pr is the Prandlt-Number and Re_p is the Reynolds-Number corresponding to the particles.

Heat transfer rate between particles and air $\dot{Q}_{p,a}$ is determined by (7), with the heat transfer coefficient $h_{p,a}$ (based on the Nusselt-Number Nu), the interfacial area per unit volume and the temperature difference between air and particles:

$$\dot{Q}_{p,a} = h_{p,a} \cdot A_{p,a} \cdot (T_a - T_p) \tag{7}$$

Radiative heat transfer is modeled with the Stefan–Boltzmann equation, assuming a wavelength independent blackbody emission.

$$E(T) = \varepsilon\sigma T^4 \tag{8}$$

with emissivity ε, $\sigma = 5.67\ 10^{-8}$ W/(m^2 K^4), and temperature T.

Thermal radiation exchange is calculated with the discrete ordinate model. This modeling approach is a compromise between accuracy and computational effort.

Transport equations for particles and fluid are coupled by source terms, which are based on the presented correlations. Integration along the particle tracks includes the source terms for the particles. The transport equations for the fluid incorporates the sources, according to the particles passing through the control volume during the actual times step.

3.5. Solar radiation

CFD simulations determine the spatial distribution of particle volume fraction for all finite volume elements. Solar source terms for the particles are calculated based on the volume fraction. Monte Carlo ray tracing provides volumetric heat sources for the discrete volumes and flux density distribution for the cavity walls. A schematic view is shown in Fig. 6. Left side of Fig. 6 shows a cross section of the cavity. To keep the computational effort low, only the volume around the particle curtain was taken into account. The inner boundary for this volume is indicated by the dashed line.

Right side of Fig. 6 shows schematically some finite volumes that are either occupied by some particles (gray) or only by air (white). Probability for a hit on a particle is based on the particle volume fraction. If a ray hits a particle, reflection or absorption occurs. Probability of absorption is equal to the emissivity of the particles, according to Kirchhoff's Law. If a ray is not absorbed, reflection takes place. Absorption or diffuse reflection can occur at the walls. This is also modeled with the probability approach. Rays are tracked until they are absorbed or they leave the cavity through the aperture.

Reflection losses are defined as the sum of rays which hit the aperture from inside the cavity. Source terms for particles are the sum of absorbed energy divided by the number of particles in a finite volume. Flux density distribution on the wall is given by the total absorbed energy on the wall faces. The spatially resolved particle heat sources and the flux distribution on the walls are fed into the CFD calculations.

3.6. Thermal radiation

Discrete ordinate model (DOM) was used for simulating thermal radiation. Basic idea of the DOM is the discretization of simulation domain in solid angle segments. To ensure an accurate enough solution, assessment of sufficient number segments has to be done. Radiative transport equation is solved for each segment of the solid angle. Radiation is assumed to be diffuse and gray (no wavelength dependent properties). Absorption of radiation in air is neglected. Radiation intensity I after passing path length s is computed by integration of thermal emission of particles and absorption by particles.

$$I(s) = \int_{s_0}^{s} (I_p - K_p I_0)\, ds' \tag{9}$$

Thermal emitted radiation I_p is the product of black body emission, particle emissivity and projected area of particles in direction of radiation. Reduction factor for incoming radiation intensity I_o is K_p, which is the absorption coefficient of particle-laden finite volumes. K_p is determined based on particle absorptivity and projected area of particles.

Usually, grid refinement for diffuse radiation simulation is much coarser than for fluid dynamic simulations. Therefore, it is possible to coarsen the grid for thermal radiation simulation. In CFX this is governed by a

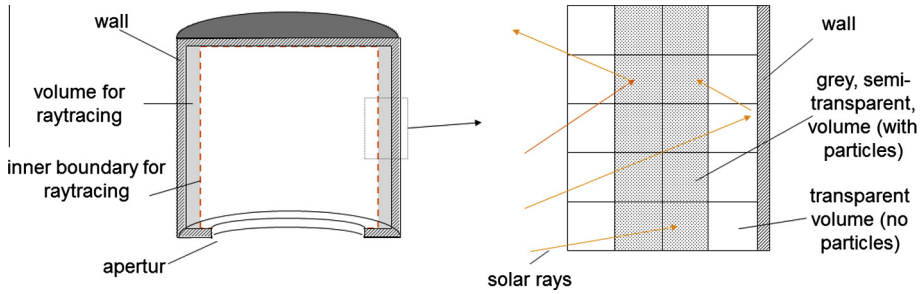

Fig. 6. Cross-section of cavity (left), schematic of ray-tracing (right). Volumes with particles are treated as semi-transparent and gray; rays can either be reflected, transmitted or absorbed in volumes; at the wall occurs either absorption or reflection.

"coarsening factor" (ratio between grid resolution for radiation to resolution for CFD simulation).

3.7. Numerical assessment

A grid study has been performed comparing four hexahedral meshes with 67,000, 178,000, 1,500,000 and 6,300,000 nodes (Fig. 7). Radiation losses were not sensitive to grid refinement in the considered range. Convective losses change with refinement. They converge to a solution, which can be extrapolated with the approach that the solution error will decrease with increasing grid refinement. Assuming that the error due to discretization is a monotone function of the number of grid elements, the exact solution (zero discretization error) can be estimated via curve fitting. Convective heat loss differs from that extrapolated value by less than 0.1%-point, with a grid size of 1.5 million hexahedral elements. Hence, this intermediate grid spacing has been proven to be sufficient.

The following convergence criteria have been considered: maximum residual lower than 10^{-4}, imbalances in equations less than 1%. Furthermore, particles outlet temperature has been observed during the simulation. Temperature fluctuations <1 K have been considered as adequate for a converged solution.

For large-scale receivers, it is not possible to solve the transport equations for all particles. For this reason only representative particles are considered. It is necessary to make sure that enough representative particles are calculated to obtain a solution, which is independent on the number of tracked particles. The adequate number of particles depends on grid refinement. Usually more particles are necessary for a finer grid, so that all finite volumes are passed by enough representative particles. This is shown schematically in Fig. 8. Left side shows particle tracks through a finite volume. In the middle only one representative particle track is determined and for a finer grid, two representative particles are necessary (right side). The representative particles have the same properties as one particle, but the coupling source terms, e.g. the heat flux to the finite volume, are multiplied with the number of particles which are represented.

A typical particle mass flow of 500 kg/s contains about one billion real particles per second. A rate of 100 000 particles per second for the intermediate grid (1.5 Mio. hexahedral elements) was found to be adequate.

Influences of coarsening factor and number of solid angle segments have been examined, to check the independence of the solution on the discretization parameters for the radiation. A grid coarsening factor of 64, with respect to the grid for fluid dynamic calculations, and a number of 8 segments have been found to be a good compromise between computational effort and accuracy. A discretization error less than 0.1%-point for the thermal radiation was accepted. Time for a simulation run was typically some hours up to some days, depending on the numerical parameters and the simulation case.

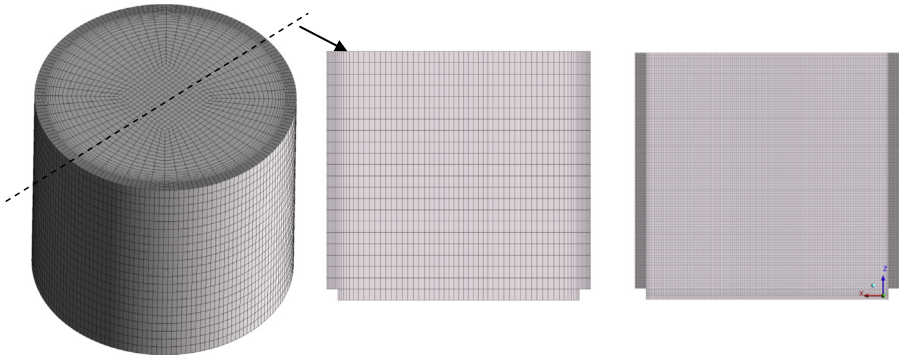

Fig. 7. 3D sketch of coarse mesh of cavity (left); middle plane coarse mesh (middle), fine mesh (right).

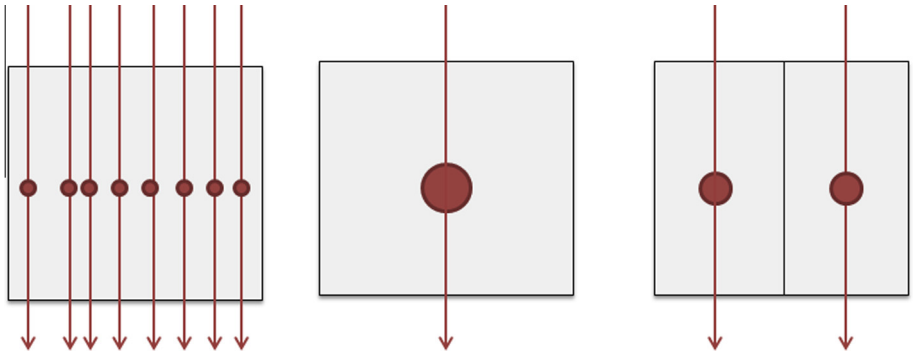

Fig. 8. Schematic of particle model; left: Euler–Lagrange method, particles are tracked through finite volume; middle: only representative particle is calculated; right: if the grid consists of more elements, more representative particles are needed, to have particles located in all finite volumes.

Monte Carlo ray-tracing was executed with 20 million rays for 1.5 million grid elements, to determine global quantities. For a detailed assessment of local quantities, at least an order of magnitude more rays are recommended.

4. Receiver efficiencies for different operational strategies

4.1. Model parameters

A receiver with a thermal output of about 350 MWth at 800 °C was chosen for first simulations, to be comparable with the simple Matlab model from Röger et al. (2011). Furthermore, the same site, heliostat field, face-down receiver geometry, and particle properties have been used. The key parameters for the model are summarized in Table 1.

Preliminary calculations showed that the simulation of particles with a medium diameter instead of particle size distribution leads to a negligible difference in simulation results. Therefore, the simulations were performed for particles with a particle size of 0.679 mm. A value of 3.56 kg/m^3 was used for particle density, following the specifications of the particle manufacturer. Emissivity of the particles was assumed to be 0.93, independent of wavelength and temperature. For specific heat capacity the correlation $-7.309\text{E}-4$ (J/kg/K^3) $T^2 + 1.608$ (J/kg/K^2) $T + 372.4$ J/kg/K was implemented (Röger et al., 2011).

Table 1
Key parameters for the modeling of the test cases corresponding to Röger et al. (2011).

Thermal output power at design point	350 MW_{th}
Design point	21.03, 12:00 h
Temperature level	300 °C → 800 °C
Site	Daggett, CA, USA, 34.5°N
Type of heliostats	121.3 m^2 glass-metal T-Type
Number of heliostats	5296
Optical tower height	309 m
Total annual heliostat field efficiency	58.1%
Aperture diameter	22.1 m
Receiver height	21.5 m

4.2. Comparison between CFD and simplified Model

Same mass flows were chosen for the CFD simulations, to be able to comparable CFD simulation with the Matlab model. Thus, the resulting particle outlet temperature is not exactly 800 °C. The average outlet temperature in the following cases is between 797 °C and 824 °C. With an adjustment of the particle mass flow the desired outlet temperature of 800 °C could be exactly reached. The work flow for the adjustment is shown schematically in Fig. 9.

A preliminary study showed that a deviation of the medium particle outlet temperature of 50 °C does not significantly affect relative losses and receiver efficiency. Therefore, no further effort was spent on adapting the medium particle outlet temperature to exactly 800 °C.

In the following, receiver losses relative to input power are compared. Receiver losses can occur due to reflection, thermal radiation, convection and conduction. Relative losses are defined as the ratio of absolute heat loss to solar input power:

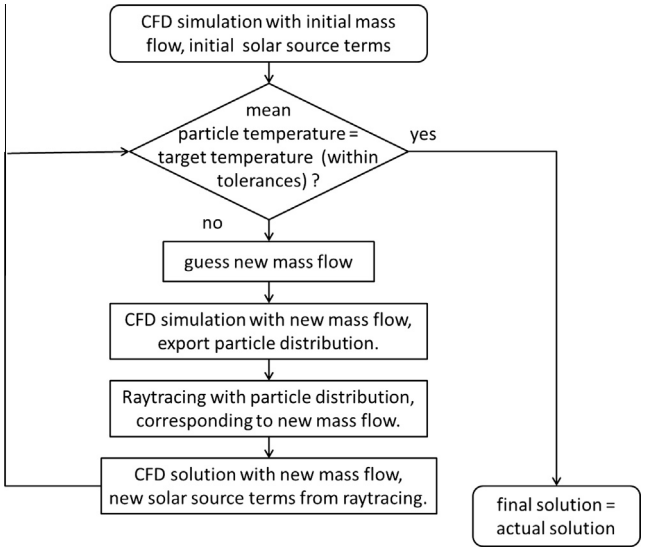

Fig. 9. Workflow for iterative calculation of the mean particle outlet temperature.

$$\dot{Q}_{loss,relative} = \frac{\dot{Q}_{loss}}{\dot{Q}_{solar\_in}}, \quad \text{e.g.relative reflection losses :}$$

$$\dot{Q}_{loss,rel,reflection.} = \frac{\dot{Q}_{loss,reflection}}{\dot{Q}_{solar\_in}} \tag{10}$$

Receiver efficiency is defined as the ratio between usable power (thermal output power) to solar input power, in other words 100% minus the sum of relative losses:

$$\begin{aligned}\eta_{receiver} &= \frac{\dot{Q}_{usable}}{\dot{Q}_{solar\_in}} = 100\% - \sum \dot{Q}_{loss,relative} \\ &= 100\% - (\dot{Q}_{loss,rel,reflection} \\ &\quad + \dot{Q}_{loss,rel,thermal\ radiation} + \dot{Q}_{loss,rel,convection} \\ &\quad + \dot{Q}_{loss,rel,conduction})\end{aligned} \tag{11}$$

Results from the Matlab model and results of the present work are compared and discussed. Fig. 10 shows results for relative losses from both models without recirculation (left side) and with recirculation (right side). The graphs show results for design point conditions (=100% load). As expected, both models show a significant decrease of reflection losses with recirculation.

However, reflection losses from the CFD model for the case without recirculation are lower than the Matlab results. It can be found that reflection losses from the different models are in rather good agreement at high particle mass flow rates, but differ by more than 10%-points at low particle mass flow rates (see Fig. 11). Different modeling of solar radiation and particle movement causes this effect. These differences are discussed in the following.

Firstly, modeling of the incoming solar radiation in the CFD model is described above. Incoming solar radiation for the Matlab model is determined by ray-tracing on absorbing faces located in front of the curtain. Radiation exchange between the curtain, the wall, and the aperture is calculated, as well as the reflection losses, based on this flux distribution and the information about transmittance of the curtain. Reflection by particle curtain is assumed to be 6%. This value was chosen for optically dense curtains and is not valid for optically thin curtains.

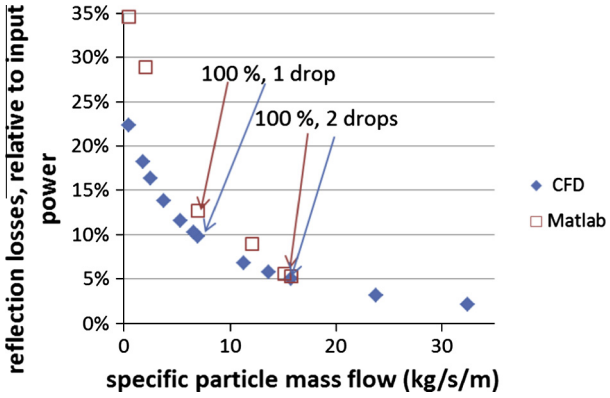

Fig. 11. Variation of the reflection losses with changes in particle mass flow.

Therefore, reflection losses are overestimated using the Matlab model for cases with low particle mass flows.

Secondly, transmittance of the particle curtain is determined in a different way. Transmittance depends on acceleration of particles, and hence on local particle velocity. Particle velocity in the Matlab model is calculated with a correlation, which assumes air velocity to be 70% of particle velocity (Röger, 2009). Air entrainment is resolved locally with the CFD model and, therefore, calculated particle velocities and volume fraction are more reliable. Typically, particle volume fraction in a hopper is about 50%. After releasing the particles, particle volume fraction decreases already in the first centimeters of fall to less than 10% due to gravity driven acceleration. In the lower part of the cavity, particle volume fraction is far below 1%. Initial particle velocity in the CFD simulations is set to 0.1 m/s. Maximal terminal velocity varies with particle mass flow because of different amounts of entrained air. This results in a maximum terminal velocity of 18.8 m/s without recirculation and 19.3 m/s with one recirculation, whereas the maximum terminal velocities obtained by the Matlab model are 14.8 m/s and 14.9 m/s for the two cases.

Convective losses are not taken into account in the Matlab model during iterative solution, but estimated

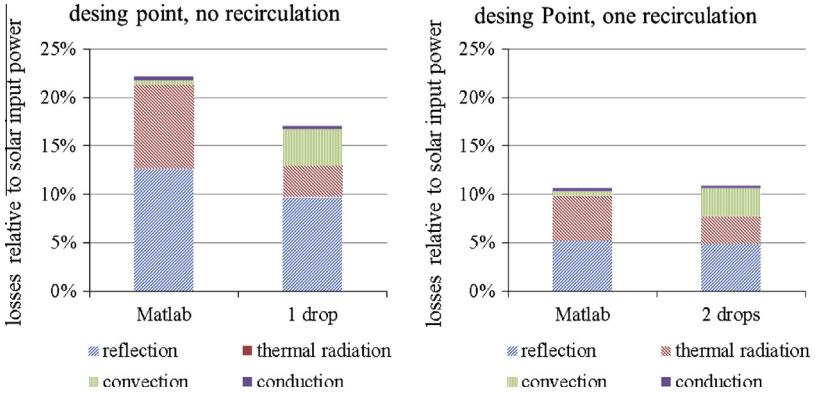

Fig. 10. Relative losses, design point (=100% load), comparison of results from Matlab model and CFD calculations; left side: 1 drop, no recirculation; right side: 2 drops, one recirculation.

Table 2
Number of drops/recirculations of particles and corresponding particle mass flows.

Number of drops through the receiver	Number of recirculations	Effective particle mass flow at receiver inlet/outlet (kg/s)	Overall particle mass flow in the cavity (kg/s)	Specific particle mass flow (per unit inlet slit length)
1	0	528	528	7.0 kg/s/m
2	1	596	1192	15.7 kg/m/s
4	3	614	2454	32.4 kg/m/s

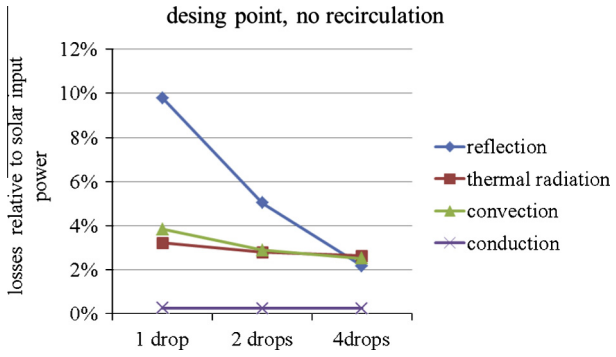

Fig. 12. Relative losses at different recirculation strategies.

Table 3
Key parameters for the modeling of the test cases corresponding to Röger et al. (2011).

Thermal output power at design point	350 MWth
Temperature level	300 °C → t800 °C
Site	Daggett, CA, USA, 34.5° N
Type of heliostats	121.3 m^2 glass-metal T-Type
Number of heliostats	5296
Optical tower height	309 m
Total annual heliostat field efficiency	58.1%
Aperture diameter	22.1 m
Receiver height	21.5 m

afterward. This results in high losses by thermal radiation. Thermal radiation and convection in the CFD model are calculated simultaneously, which is physical reality. Convective cooling of particles and walls leads to a reduction of temperatures of particles and walls, and so to lower radiation losses in comparison to the Matlab results. On the other hand, convective heat transfer from particles and walls to the surrounding air leads to higher air temperature in the receiver, and thus to higher convective losses through the aperture. So, thermal radiation losses calculated with the Matlab model constitute more than 90% of total thermal losses, whereas according to the CFD model they are responsible for slightly less than 50 % (Fig. 10). In total, overall efficiency with no recirculation is 5.1%-points higher according to the CFD model calculations and 0.2%-points lower with four drops, in comparison to the Matlab model.

4.3. Effect of Recirculation on Receiver Efficiency

Effect of particle recirculation was assessed by a set of simulations with 1, 2 and 4 drops of the particles. The corresponding particle mass flows are summarized in Table 2.

Receiver efficiency from the CFD model was 83% in the design point without recirculation. With an improved operational strategy, simulations indicate efficiency increases to 89% with one recirculation, and efficiency in excess of 92% with three recirculations.

Efficiency increase with increasing number of recirculations is mainly due to reduced solar reflection losses from almost 10% down to 2.2% (see Fig. 12). Convective losses add up to 3.8% without recirculation and decrease slightly

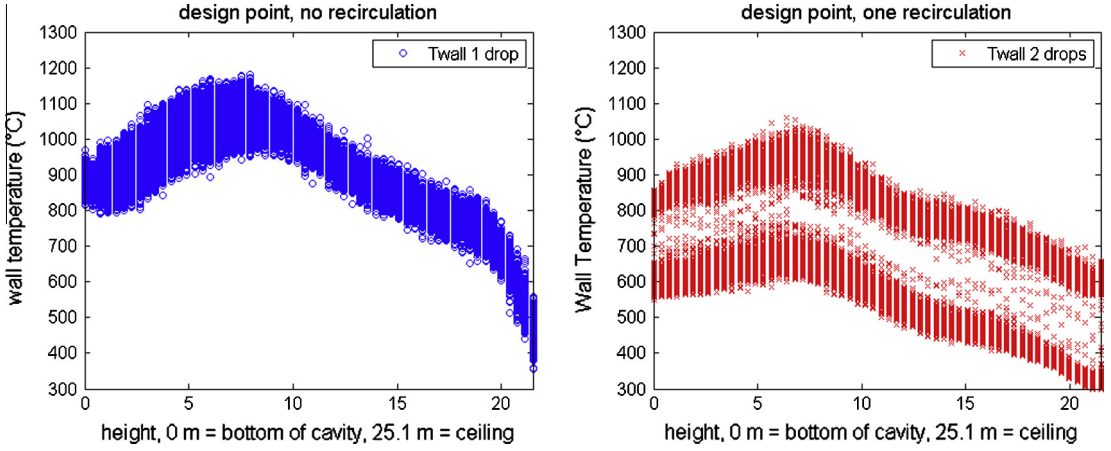

Fig. 13. Wall temperatures without recirculation (left) and with one recirculation (right).

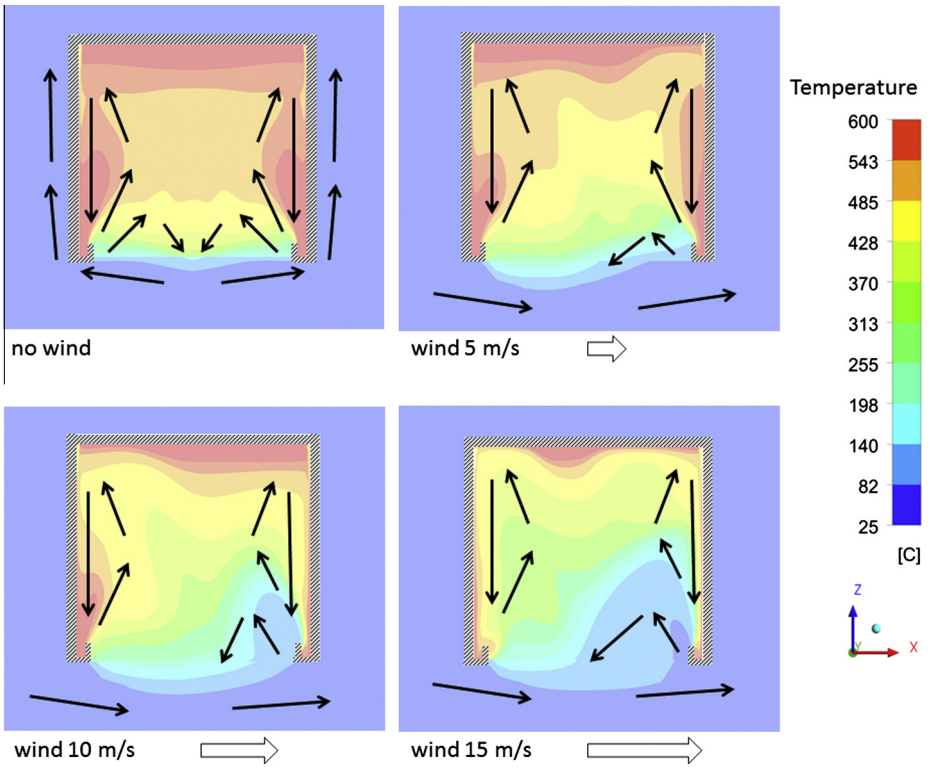

Fig. 14. Flow field in middle plane for different cases: no wind and with horizontal side wind, wind speeds 5 m/s, 10 m/s and 15 m/s.

with increasing particle mass flow, because of lower radiative and conductive heat losses from the walls, associated with lower wall temperatures.

Wall temperatures both cases are shown in Fig. 13. On the right side the case without recirculation is displayed. Wall temperature is shown as a function of height. Maximum wall temperature is in the lower third of the cavity, where the highest solar flux is on the walls. This is due to the incoming radiation and to the fact that optical density of the particle curtain is lower at the bottom. Spread of temperature values at one height is due to the variation of incoming radiative flux at different circumferential positions in the cavity. A similar distribution appears for the case with one recirculation (Fig. 13, right side). However, temperatures are generally lower, because of optically denser particle curtain, and therefore lower solar fluxes on the wall. On south side of the cavity, where first drop of particles takes place, particle temperatures are lower than on north side of the receiver (second drop). Hence, heat transfer from particles to walls is different for the two particle sections, and leads different wall temperatures and an obvious division of the temperature spread over circumference, which is a significant difference between these cases.

Thermal radiation losses were calculated to be 3.2% for the one drop case. With increasing mass flow they decrease by 0.6%-points. This is attributed to the lower wall temperature. Conduction losses contribute only a small amount between 0.2% and 0.3%.

5. Wind effects

5.1. Model parameters

Wind influence was assessed with the same model parameters (Table 3). In addition, an inlet boundary condition was implemented to simulate side wind. Wind was assumed to be horizontal and wind speeds up to 15 m/s were taken into account. According to the logarithmic wind law, this corresponds to a ground wind speed of 9 m/s. Heliostat fields normally switches to stow position with mirrors parallel to the ground above this wind speed. Four cases have been simulated: the reference case with no wind and three cases with side wind at three different wind speeds (5 m/s, 10 m/s and 15 m/s), with 2 drops, i.e. one recirculation. Again, as input power and mass flow have been kept constant, outlet temperature varied only between 760 °C and 780 °C, which was close enough to be comparable, and therefore no further adjustment of the particle mass flow was required.

6. Results

In Fig. 14 temperature (color)[1] and flow fields (arrows) in the middle plane of the simulated cases are shown.

[1] For interpretation of color in Fig. 14, the reader is referred to the web version of this article.

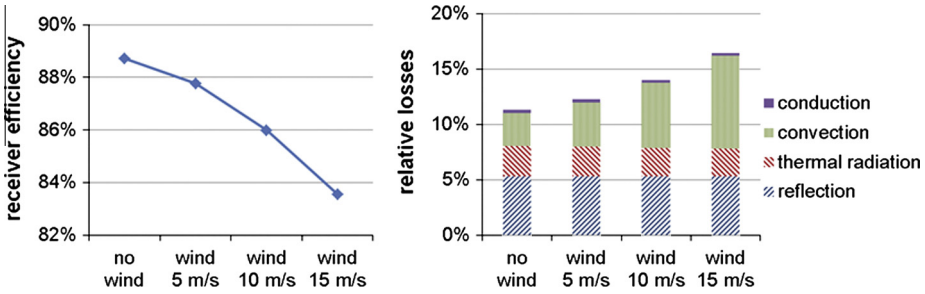

Fig. 15. Receiver efficiency depending on wind velocity (left) and relative losses depending on wind velocity (right).

Particle tracks are not plotted. They are located quite close to the edges of the cavity, and cause downwards acceleration of the air.

For the case with no wind, it is obvious that the air is heated by walls and particles and, therefore, reaches the highest temperatures in the lower part of the receiver, close to the walls. Hot air rises in the cavity and forms a stagnation zone (layering of hot air above colder air layers) and forms a hot zone at the ceiling. At the bottom, at the open aperture, the surrounding air is also heated. Parts of the heated air rise along the outer walls of the cavity. Heat losses caused by this buoyancy driven convection are the convective losses of the receiver. If wind occurs, this free convection is overlaid with forced convection caused by wind flow.

Side wind from left side enters the cavity at the right edge (in Fig. 14), forms a vortex, and leaves the cavity near the middle of the aperture. At low wind speeds, flow field is not much affected. With increasing wind speed from 5 m/s to 10 m/s vortex height increases from about one third to half of cavity height. As wind speed was increased to 15 m/s vortex height did not increase significantly, but the width.

This vortex leads to a decrease of efficiency, due to an increase in convection losses. Receiver efficiency reaches up to 89% without wind and is reduced to 84% in case of 15 m/s side wind (Fig. 15, left). The graph on the right side of Fig. 15 shows a breakdown of different losses. Reflection, conduction and thermal radiation losses are not significantly affected by wind. However, convection losses are 3.0% without wind, and more than twice as much in case of 15 m/s wind speed. In this case the increase was 5.4%-points.

7. Conclusions and outlook

A particle receiver is a promising concept for increasing system efficiencies of solar tower power plants. Receiver efficiency can be determined with the developed advanced model. The CFD model provides more detailed information about physical effects, radiation and heat losses, compared to previous models. Thermal radiation losses predicted by the CFD model are significantly lower than estimated by the Matlab screening model. Convection losses are higher compared to the Matlab model.

First results confirm the results of previous calculations of receiver efficiencies, especially the fact that recirculation can increase receiver efficiency due to the decrease of reflection losses. Receiver efficiency in excess of 92% is predicted for operation with three recirculations,

Gain in receiver efficiency due to recirculation has to be compared with additional effort for transport of the particles, to assess economical potential. This has not been assessed yet, but is in focus of future research.

Interaction with the surrounding is included more adequately compared to previous model approaches. Therefore, influence of wind can be assessed. Side wind increases the convection losses significantly, due to vortex generation. To evaluate the possibility of reduction of convention losses, the authors propose assessment of a wind shield.

Beyond theoretical assessment, focus of future work will be validation of the complete CFD model with experimental data.

References

ANSYS Inc: ANSYS CFX-Solver Modeling Guide, Release 12.0, 2009.

Buck, R., Teufel, E., 2009. Comparison and optimization of heliostat canting methods. J. Sol. Energy Eng. 131 (1).

Crowe, T.C., Tsuji, Y., Sommerfeld, M., 1997. Multiphase Flows with Droplets and Particles. CRC Press LLC, Florida.

Falcon, P.K., Noring, J.E., Hruby, J.M., Assessment of a Solid Particle Receiver for High Temperature Solar Central Receiver Systems. 1985, Sandia Report SAND85-8208.

Falcone, P.K., Noring, J. E., Hackett, C. E.,1982. Evaluation and Application of Solid Thermal Energy Carriers at High Temperature Solar Central Receiver System. In: Proc. IECEC '82 17th Intersociety Energy Conversion Engineering Conference.

Grena, R., 2009. Thermal simulation of a single particle in a falling-particle solar receiver. Sol. Energy 83 (8), 1186–1199.

Griffin, J.W., Stahl, K.A., Petit, R.B., 1986. Optical properties of solid particle receiver materials: I. Angular scattering and extinction characteristics of Norton Masterbeads. Solar Energy Mater. 14, 395–416.

Ho, C., Röger, M., Khalsa, S., Amsbeck, L., Buck, R., Siegel, N., Kolb, G., 2009. Experimental validation of different modeling approaches for solid particle receivers, In: Proceedings of the SolarPACES Conference, Berlin, Germany.

Jukkola, G.; Turek, D.; Levasseur, A.; Teigen, B. Operating experience with ALSTOM's circulating moving bed combustor. In: 17th

International Conference on Fluidized Bed Combustion, May 18–21, 2003, Jacksonville, Florida, USA.

Kim, K., Moujaes, S.F., Kolb, G.J., 2010a. Experimental and simulation study on wind affecting particle flow in a solar receiver. Sol. Energy 84 (2), 263–270.

Kim, K., Siegel, N., Kolb, G., Rangaswamy, V., Moujaes, S.F., 2010b. A study of solid particle flow characterization in solar particle receiver. Sol. Energy 84 (2), 263–270.

Leary, P.L., Hankins, J.D.. A User's Guide for MIRVAL – a computer code for comparing designs of heliostat-receiver optics for central receiver solar power plants. In: Sandia Laboratories Report, SAND77-8280, 1979.

Menter, F., Carregal, J., Esch, T., Konno, B.,2003. The SST turbulence model with improved wall treatment for heat transfer predictions in gas turbines. In: Proceedings of the International Gas Turbine Congress 2003 Tokyo.

Röger, M., Amsbeck, L., Buck, R., Gobereit, B., 2011. Face-down solid particle receiver using recirculation. J. Sol. Energy Eng. 133, 031009.

Schwarzbözl, P., Pitz-Paal, R., Schmitz, M., 2009. Visual HFLCAL – a software tool for layout and optimisation of heliostat fields. In: Proceedings. SolarPACES 2009, 15.-18.September 2009, Berlin.

Siegel, N., Ho, C., Khalsa, S., Kolb, G., 2010. Development and evaluation of a prototype solid particle receiver: on-sun testing and model validation. J. Sol. Energy Eng. 132, 021008.

Tan, T., Chen, Y., Chen, Z., Siegel, N., Kolb, G.J., 2009. Wind effect on the performance of solid particle solar receivers with and without the protection of an aerowindow. Sol. Energy 83 (10), 1815–1827.

VDI-Heat Atlas. Springer, 10. Auflage, 2006.